Materials Science & Engineering A 607 (2014) 445–453

Contents lists available at ScienceDirect

Materials Science & Engineering A

journal homepage: www.elsevier.com/locate/msea

Microstructure-properties correlation in fiber laser welding of dual-phase and HSLA steels

D.C. Saha [a,*], D. Westerbaan [a], S.S. Nayak [a], E. Biro [b], A.P. Gerlich [a], Y. Zhou [a]

[a] Department of Mechanical and Mechatronics Engineering, University of Waterloo, 200 University Avenue West, Waterloo, ON, Canada N2L 3G1
[b] ArcelorMittal Global Research, 1390 Burlington Street East, Hamilton, ON, Canada L8N 3J5

ARTICLE INFO

Article history:
Received 1 March 2014
Received in revised form
4 April 2014
Accepted 7 April 2014
Available online 16 April 2014

Keywords:
Fiber laser welds
Microstructure
Transmission electron microscopy
Nanoindentation
Tensile testing
Microhardness

ABSTRACT

Similar and dissimilar welds of dual-phase (DP) and high strength low alloy (HSLA) steels were made by fiber laser welding (FLW). The welds were characterized with respect to microstructure, micro- and nano-hardness, and tensile properties. The fusion zone (FZ) in the DP welds consisted of fully martensitic structure; whereas HSLA and dissimilar weld FZ microstructure were mixture of martensite and bainite. Analytical transmission electron microscopy (TEM) confirmed bainite structures containing bainitic ferrite laths with intralath and interlath cementite. Precipitation of single variant carbides inside the bainitic ferrite laths were confirmed by measuring the interplanar spacing. The cooling rate in the FZ, estimated using Rosenthal equation, and continuous-cooling-transformation diagrams corroborated the microstructure formed. Nanoindentation was used to verify the hardness of these individual micro-constituents, since a much lower nano-hardness for bainite (4.11 GPa) was observed compared to martensite (6.57 GPa) phase. Tensile failure occurred in the tempered area of the heat affected zone (HAZ) in the DP steel welded, which was confirmed by typical cup-like dimple fracture; likewise failure in the HSLA base metal, which occurred in dissimilar and HSLA welds, indicated distinctive dimple and shear dimple ductile morphology.

1. Introduction

Fuel efficiency, safety, and environmental impact are key issues for the automotive industry [1,2], which can be accomplished with the use of advanced high strength steel (AHSS) as a result of high strength and good formability. In terms of design flexibility, DP steel offers one of the highest combinations of strength and ductility compared to other AHSS grades [3]. The microstructure of a DP steel consists of soft ferrite matrix embedded with harder secondary phase i.e. martensite and/or bainite [4]. The volume fraction of martensite determines the strength and grade of the DP steel. For example, DP600 grade represents steel with minimum ultimate tensile strength (UTS) of 600 MPa and similarly the other grades DP780, DP980, and DP1100 represents steel with minimum UTS of 780 MPa, 980 MPa and 1100 MPa, respectively. Although use of DP steel in the auto industry is rapidly increasing, high strength low alloy (HSLA) steel is still predominately used in structural applications for manufacturing automotive parts because many applications are stiffness driven, and the modulus of elasticity values of steels are nearly constant. However, some applications require higher elongations than those feasible with HSLA or superior strength compared to low carbon steel and other conventional heat-treated automotive steels [5]. In addition, due to the lower alloy content HSLA also has better weldability [6] compared to high alloy content DP steel. There are numerous applications where multi-materials are tailored to meet local requirements of the joint [7]. In the case of DP steel welds high strength with lower ductility is achieved, meanwhile HSLA provides excellent ductility with low strength. Therefore, achieving high strength with reasonable ductility would be highly desirable when laser welded blanks (LWBs) are produced by introducing multi-materials combinations [8–10]. The performance of the welds is strongly influenced by the post-weld microstructure [11]. Martensite phase in DP steel is tempered during welding and results in reduction of hardness in the tempered region of the heat affected zone (HAZ), a phenomenon generally known as HAZ softening. HAZ softening has detrimental effects on the weld properties with strain localization in the tempered region of the HAZ at lower stresses than may be supported by the base material (BM) [12–14].

Increasing the use of laser welded blanks (LWBs), also known as TWBs, is another way auto makers are decreasing vehicle weight to reduce CO_2 emission and increase fuel economy. LWBs are composed of two or more sheets of similar or dissimilar materials, thicknesses and/or coating types welded together, which are formed to fabricate the required three dimensional automotive body parts [15]. The advantages of LWBs include weight reduction, cost minimization,

* Corresponding author. Tel.: +1 226 606 0119 (Cell), +1 519 888 4567x35625 (Office); fax: +1 519 888 6197.
E-mail address: dcsaha@uwaterloo.ca (D.C. Saha).

http://dx.doi.org/10.1016/j.msea.2014.04.034
0921-5093/

improved material usage, and scrap reduction with improved part integration. Generally, LWBs are made with mild or interstitial free (IF) steels; however, in recent years the weight reduction ability of LWBs have been increased by employing high strength steels like HSLA steel and AHSS which also improves the crash performance of the blanks, since higher strength alloys can be used in the location which are most critical [16–18]. This implies that dissimilar steel combinations will be encountered.

Initially, the automotive industry relied on CO_2 lasers to make LWBs; however, recently fiber laser welding (FLW) has gained popularity because of its several advantages e.g. lower capital costs, higher plug efficiency, greater flexibility in beam delivery, higher power density ($>10^5$ W/cm^2), narrower beam size (<10 μm) thus producing welds with improved properties [12,13]. In addition, high speed welding can be performed in FLW, which eventually increases the productivity and reduced production cost. Higher welding speeds are also advantageous in terms of the HAZ softening due to reduction in its severity and the soft zone width [12,13].

There have been reports on the DP steel welds produced by different welding processes like resistance spot welding (RSW), diode laser welding, arc welding, and flash welding [19–24]. However, the author's recent studies indicated that FLW is beneficial in producing LWBs compared to other welding processes [12–14,25]. These studies [12–14,25] were focused on similar welds and on microstructural evaluation within the FZ were not closely examined. This study attempts to fill this gap by reporting the evolution of microstructure within the FZ and its consequence effects on mechanical properties of DP and HSLA steel sheets joined by FLW in both similar and dissimilar materials combinations.

2. Experimental procedure

All experiments were conducted on 1.2 mm thickness of hot dip galvanized (HDGI) DP980 (UTS ≥ 980 MPa) and HSLA (UTS ≥ 500). The chemistry and mechanical properties of the steels are shown in Table 1. Welds were made using an IPG Photonics Ytterbium Fiber Laser System (YLS-6000-S2), the details of which are listed in Table 2. The steels were fiber laser welded using the same welding procedures reported in previous studies [14]. Fiber laser welds were made on butt welding configuration with laser power of 6 kW, welding speeds 12, 14, and 16 m/min, and beam focal length of 200 mm. Microstructural characterization and microhardness measurements were carried out on weld cross-sections prepared using standard metallographic procedures followed by etching with 2% Nital solution. A JEOL JSM 6460 scanning electron microscope was used for characterizing the microstructure. Vickers microhardness was measured in a Clemex JS-2000 automated computerized hardness tester under 200 g load and 15 s dwell time. Sufficient distance (150 μm) was maintained between consecutive indentations to avoid interference from the stain fields developed by the adjacent indents. Nanoindentation was performed on the etched specimens using 4000 μN load for 20 s in a Hysitron Triboindenter TI-900 equipped with scanning probe microscope. Prior to running actual tests the instrument was calibrated by indenting a fused silica reference specimen. TEM study was performed in a PHILIPS CM12 microscope by analyzing the electron transparent specimens prepared by twin-jet electropolishing 3 mm diameter discs of thickness below 60 μm. Transverse tensile specimens were machined as per standard (ASTM: E8/E8M) [26] with the sample dimensions shown in Refs. [12,13]. The tensile tests were carried out using a fully computerized Instron tensile testing machine at a stain rate of 0.001/s. The fractography studies of the tensile tested samples and the nano indents in the specimens were done in a Zeiss LEO 1550 field emission scanning electron microscope.

3. Experimental results

3.1. Microstructure

The representative microstructure of the BM of DP980 steel consisted of a ferrite (F, dark regions) and martensite phase (M, white regions) (Fig. 1(a)). The BM of the HSLA steels consisted of a ferrite matrix (F) with carbides (C) distributed inside the grains or along the grain boundaries (Fig. 1(b)). Fig. 2 shows the weld profile of the dissimilar DP980 and HSLA weld; different microstructural regions are marked as b and c for subcritical heat affected zone (SCHAZ), and intercritical HAZ (ICHAZ) at the DP980 steel side, d for centerline of the FZ, and e, f for super-critical zone, and ICHAZ at the HSLA side. The tempered region on the DP980 side of the weld (Fig. 2(b)), also known as SCHAZ, was observed next to the BM illustrating carbide precipitation at the lath boundaries and the prior-γ grain boundaries, which agrees with the literature [12–14,22,24,27–30]. In the ICHAZ (Fig. 2(c)), the newly formed martensite (marked as NM) seen is the transformation product of rapidly cooled and nucleated austenite along the grain boundaries of the ferrite or at the ferrite/martensite interfaces. It should be noted that the microstructure (Fig. 2(c)) contained a lower fraction of martensite compared to the BM (Fig. 1(a)). This is attributed to local incomplete austenitization resulting from the high heating rate involved in the FLW. The center of the FZ showed a mixed microstructure containing martensite and bainite (Fig. 2(d)), which was consistent near the weld centerline. The super-critical zone on the HSLA side of the weld (Fig. 2(e)) contained martensite and bainite microconstituents as the transformation products of austenite, which was formed when the steel was heated in excess of to the Ac_3 temperature. The microstructure of the ICHAZ (Fig. 2(f)) on the HSLA steel side contained ferrite, carbides, and martensite, which was identical to the microstructure observed in the ICHAZ in similar HSLA fiber laser welds [14]. The SCHAZ of the HSLA side of the weld could not be identified metallographically, as the HSLA is more thermally stable than the DP980, and therefore does not have microstructure that is distinct from its BM.

3.2. Mechanical properties

3.2.1. Microhardness

The microhardness profiles for all the welds are compared in Fig. 3. The hardness profile within the FZ of the dissimilar weld was observed to be in-between that of the similar welds; with an increased hardness value on the HSLA side of the FZ compared to the similar HSLA weld; this is also evidence of lack of mixing. This

Table 1
Chemical composition and mechanical properties of the materials used in this investigation.

Steel	C	Mn	Mo	Si	Cr	Al	Ni	V	Fe	YS (MPa)	UTS (MPa)	Elongation (%)
DP980	0.15	1.5	0.0	0.3	0.0	0.05	0.0	0.00	Bal.	719	1097	12.9
HSLA	0.08	0.8	0.0	0.5	0.0	0.05	0.0	0.00	Bal.	401	548	20.0

Table 2
Fiber laser characteristics used in this study.

Laser type	Laser source		Laser head		Beam	Fiber
	Make	Model	Make	Focal length	Spot size	Fiber core
Ytterbium Laser System	IPG photonics	YLS-6000-S2	Laser mechanisms	200 mm	0.6 mm diameter	0.3 mm diameter

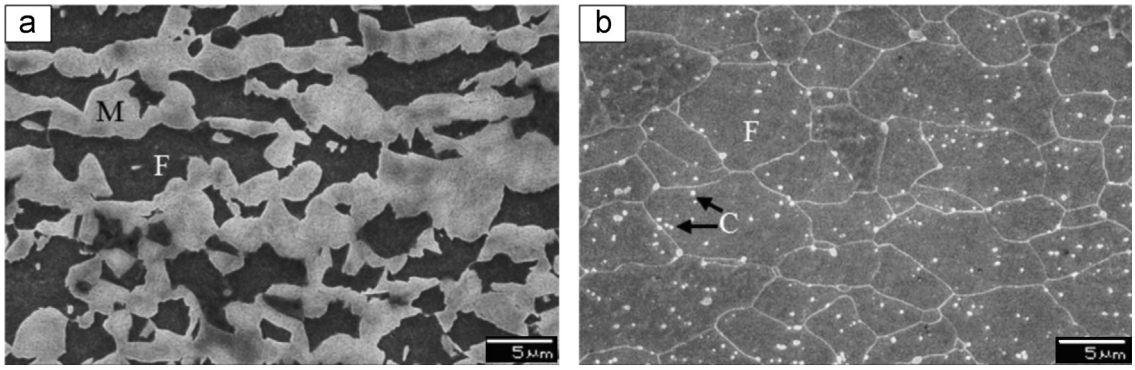

Fig. 1. Typical microstructure of the as-received materials (a) DP980, and (b) HSLA steel; where F is ferrite, M is martensite, and C is carbides.

phenomenon can be attributed to richer chemistry formed by mixing of the materials resulting in the formation of a higher martensite fraction upon cooling to the room temperature. The elemental compositions were carried out by energy-dispersive x-ray spectroscopy (EDX) line scanning to estimate the Mn concentration along the FZ for three kind of welded samples. The average Mn concentrations were measured to be (in wt%) about 1.58, 1.22, and 0.84 for similar DP980, dissimilar, and similar HSLA weld, respectively. The estimated Mn concentration also confirmed the presence of richer chemistry formed by mixing of two dissimilar materials as expected. The FZ hardness of the DP980 weld was observed to be higher when compared to HSLA weld and dissimilar weld due to the fully martensitic microstructure [14]. It is interesting to note that a hardness reduction was detected in the FZ on the DP980 side just beside the weld centerline; which was attributed to the formation of the softer microstructure containing bainite (Fig. 2(d)) [31]. In addition, the hardness at the centerline of the FZ in the dissimilar weld was close to that of the similar HSLA weld consisting of bainite and martensite [14]. The hardness in the SCHAZ, which is marked as soft zone (circles) in Fig. 3, was found to be 50 HV below the hardness of the DP980 steel sheet. Softening in the DP980 steel welds is attributed to martensite tempering, which occurs when the steel is heated between 300 °C and its Ac_1 temperature [27,32,33]. The minimum hardness of this softened zone varied from 303 to 288 HV, which increased with increasing welding speed, while the FZ also became narrower (0.8–0.6 mm). However, the FZ width in all the welds, as measured from the hardness profiles, was in the range of 800–900 μm [14]. The width of the HAZ and the FZ is dependent on the welding parameters used and also the welding process [14].

3.2.2. Tensile properties and fractography

The engineering stress vs. engineering strain curves of the BM and the welds of DP980 and HSLA steel are shown in Fig. 4. The base metal of the DP980 steel exhibits the highest ultimate tensile strength (UTS, 1097 MPa) and elongation (12.9%) as expected; alternatively, the BM shows minimal yield strength (YS, 719 MPa) compared to welded samples (Table 3). Increasing welding speed from 12 m/min to 16 m/min decreased the UTS from 1081 MPa to 1041 MPa; although YS remained nearly same as that of the BM. It can be noted here that the YS of the SCHAZ may increase the YS as the upper yield strength (UYS) and lower yield strength (LYS) characteristics return [34,35]; but due to sample geometry, it was not measured as the BM was yielded first. The mechanical properties of the welded specimens demonstrated a reduction from the BM properties. During the tensile test, it was observed that the fracture occurred in the SCHAZ (Fig. 5(a)); which can be predicted from microhardness distributions as hardness values were significantly lower in this zone (Fig. 3). Necking was not seen in the BM of the fractured specimen, and the heterogeneity of the sample likely contributed to the decrease in the ductility, with a lower load bearing capacity of the soft zone where failure occurred. It can be asserted here that the ductility of the SCHAZ would be much higher than that of the BM in case of DP980 steel [34,35]. However, as strain was highly localized in the SCHAZ and not over the entire gauge length, elongation appeared to decrease.

In contrast to DP980 steel, the joint efficiency and elongation of the HSLA welds were not influenced by the welding speed (Table 3), these welds consistently fractured in the BM, which suggested that strain localization occurred in the BM because the weld area had a higher hardness than the unaffected BM. This can be inferred from the hardness distribution pattern (Fig. 3); in contrast to the DP980 steel welds, there is no softened zone found in the HSLA steel welds; the hardness values throughout the HAZ were much higher than those of the BM. Fracture occurred in the BM away from the center of the FZ in similar HSLA welds (Fig. 5(b)). Prior to fracture, extensive necking and elongation was observed, eventually failure occurred at one side of the weldment.

For the dissimilar welds, tensile failure occurred in the HSLA BM (Fig. 5(c)), as in the case of the similar HSLA weld (Fig. 5(b)). This was attributed to the lower BM strength of HSLA, which was the weakest area of the dissimilar weld, and exhibited lower hardness values than the SCHAZ on the DP980 side of the joint (Fig. 3). The DP980 steel similar weld exhibited greater YS and UTS compared to the similar HSLA and dissimilar welds; however, the dissimilar welds demonstrated slightly higher YS and achieved the material UTS at lower elongation values as half of the joints were yielded, with a reduction in the elongation compared to the HSLA similar welds. However, the UTS of the dissimilar weld was close to that of the HSLA welds; because the DP980 steel side of the weld did not yield and so the plastic deformation only occurred in the HSLA side of the weld, resulting in the decrease in the elongation when compared to the HSLA–HSLA welds. The

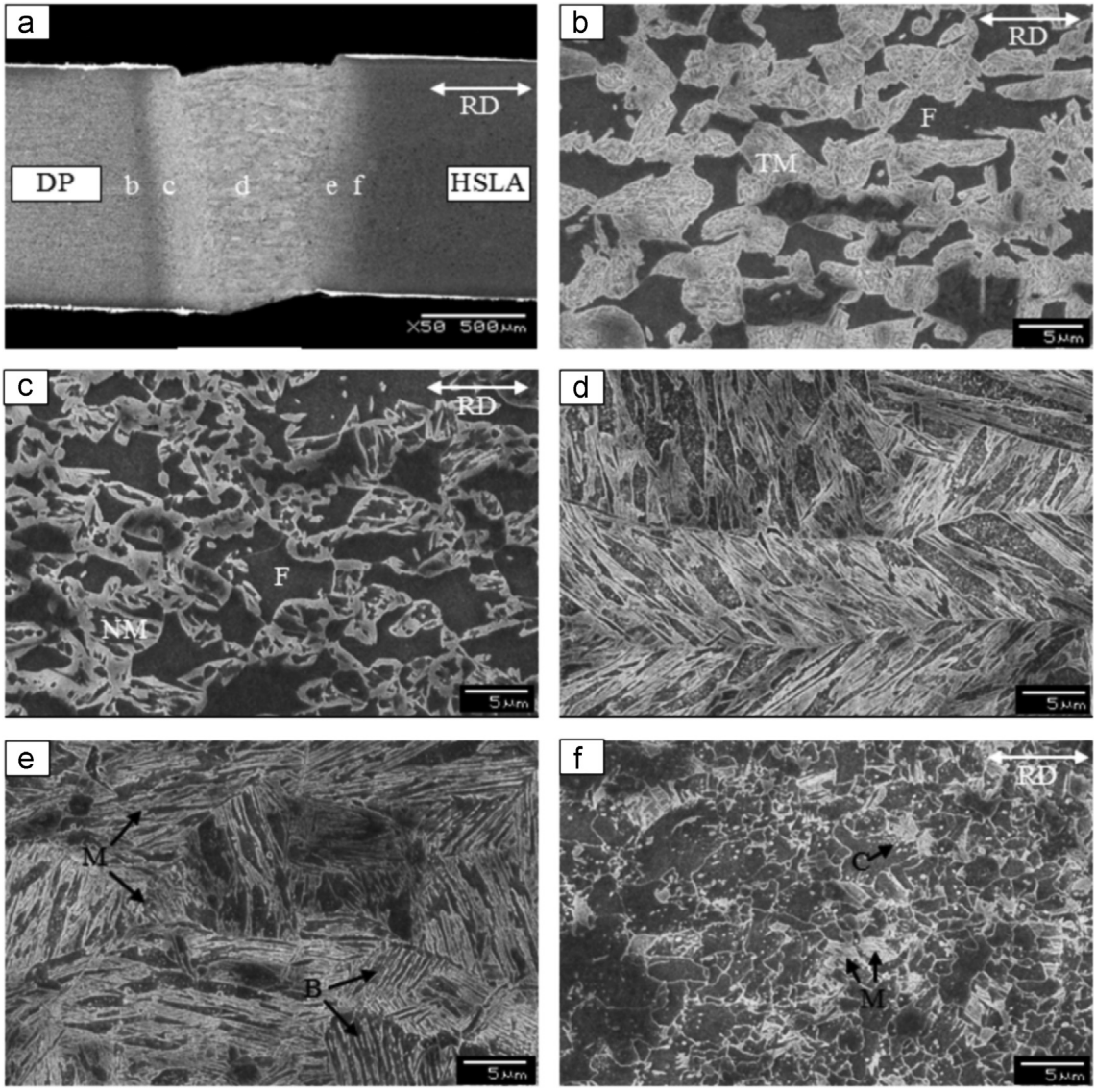

Fig. 2. SEM micrographs of DP980-HSLA steel dissimilar weld (6 kW power and 16 m/min speed) showing (a) the full weld profile, (b) SCHAZ in DP980 side, (c) the ICHAZ in DP980 side, (d) the FZ, (e) the super-critical HAZ in HSLA side, and (f) the ICHAZ in HSLA side; where F is ferrite, M is martensite, TM is tempered martensite, NM is newly formed martensite, C is carbides, and B is bainite.

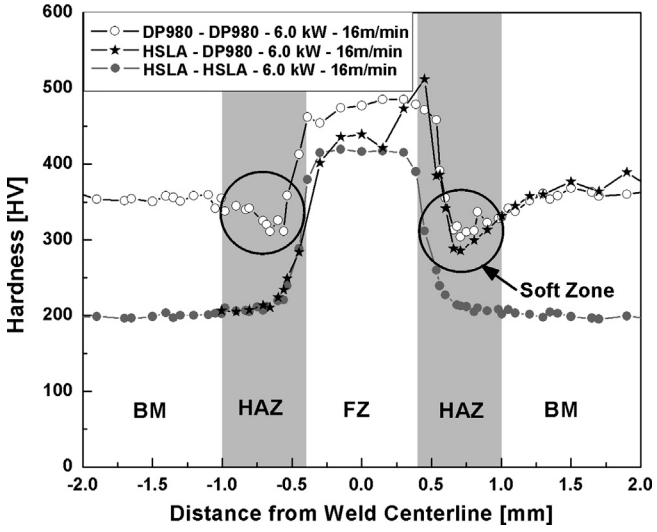

Fig. 3. Representative hardness profiles across the similar DP980, HSLA, and a dissimilar HSLA-DP980 weld.

representative SEM images of the fracture surfaces are presented in Fig. 6. The fracture surfaces of the DP980 steel welds (Fig. 6(a)) and dissimilar welds (Fig. 6(b)) showed ductile failure with distinctive cup-like dimples. It should be noted that the dissimilar welds fractured in the HSLA BM, as in the case of HSLA similar welds.

4. Discussions

4.1. Effect of chemistry on the FZ microstructure

As discussed earlier, the FZ of the dissimilar weld was composed predominantly of martensite with a bainitic structure; the distribution of structures within the FZ depends on the cooling rate associated in FLW process. Nd:YAG laser welds (very similar to FLW) have high cooling rates; the normal cooling rates range is about 10^3–10^5 °C/s [27]. The Rosenthal equation was used to estimate the cooling rate within the FZ in the FLW [36], based

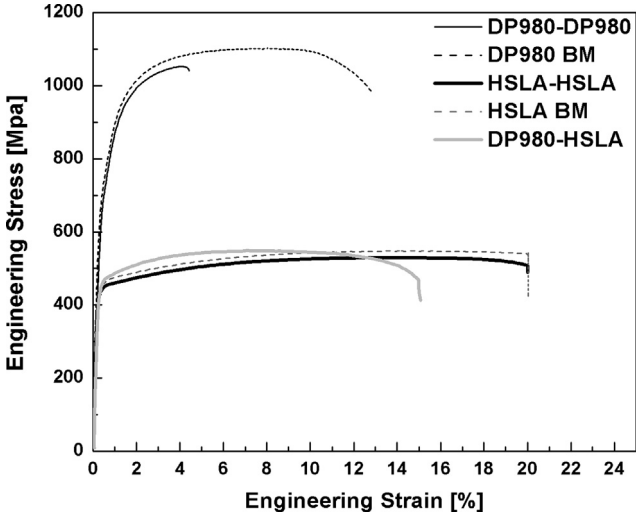

Fig. 4. Representative engineering stress versus engineering strain of the DP980 and HSLA base materials, as well as similar and dissimilar combination fiber laser welds (made using 6.0 kW, 16 m/min) tested at a strain rate of 0.001/s.

Table 3
Mechanical properties for single linear FLW of DP980, and HSLA steels of different welding speeds.

Steel	Weld type	Welding speed [m/min]	Yield strength [MPa]	Ultimate tensile strength [MPa]	Elongation [%]	Joint efficiency [%]
DP980	BM	–	719	1097	12.9	–
	Welded	16	725	1041	4.7	95
		14	721	1085	4.8	99
		12	736	1081	3.9	99
HSLA	BM	–	401	548	20.0	–
	Welded	16	404	530	20.0	98
		14	414	538	20.2	98
		12	412	534	20.0	98

on the following relation,

$$\frac{\partial \Theta}{\partial t} = -\frac{2\pi k_s^2}{\alpha}\left(\frac{\upsilon \Delta x}{Q}\right)^2 (\Theta - \Theta_0)^3 \quad (1)$$

where $\partial\Theta/\partial t$ is the cooling rate, k_s is the thermal conductivity of the steel (30 W/m/K), α is the thermal diffusivity of the steel (5.613×10^{-6} m^2/s), υ is the welding speed (m/s), Δx is the sheet thickness (mm), Q is the power input (J/mm^2), Θ, and Θ_0 are temperature (K) of the weldment (1798 K) and the ambient temperature (298 K), respectively. The corresponding values and constants of the parameters indicated in Eq. (1) were taken from the literature [27]. Using Eq. (1), the cooling rate in the FZ was estimated to be about 10,000 K/s; which is consistent with values reported in earlier work [27,36]. This cooling rate was sufficient to form fully martensitic structure in the FZ. In addition, the DP980 steel used in this study contained high C and Mn content (Table 1), leading to high hardenability by delaying the ferrite and bainite formation thus increasing the critical cooling rate [36]. Therefore, it is reported that the rapid cooling rate (about 10,000 K/s) in FLW coupled with higher hardenability of the DP980 steel formed a FZ with fully martensitic structure.

In contrast to DP980 steel, HSLA steel formed a FZ microstructure with a mixed microstructure containing bainite and martensite, which is attributed to the lower hardenability of the steel because of the lower alloying additions compared to the DP980 steel (Table 1). Mn is an austenite stabilizer and thus lowering Mn content prompts ferrite formation at lower cooling rate; however, the cooling rate in FLW was too rapid for ferrite nucleation resulting in the observed bainitic/martensitic microstructure. This can be better explained by referring to the calculated CCT curve (note that the calculated CCT curve for dissimilar weld was done based on 50:50 fraction mixed in the FZ) of the investigated steels (Fig. 7), the bainite nose shifts to the right of the curve when more alloying additions are added to the steel. Therefore, due to a lower alloying addition and rapid cooling (about 10,000 K/s), the cooling curve can intersect the bainite nose to form a small fraction of bainite along with the predominantly martensite matrix in HSLA and dissimilar welds [37].

The microstructure containing martensite and bainite microconstituents were detected along the centerline of the dissimilar welds (Fig. 2(d)). As discussed in earlier sections, the HSLA side of the FZ consisted of bainite and martensite phase; whereas the DP980 side of the FZ was expected to form a similar microstructure due to the mixing of molten steels in the weld pool. The chemistry within the FZ of a dissimilar weld is theoretically considered as the average of those of the corresponding BM considering that the metal was not lost from the weld pool [23]. Furthermore, the cooling rate was same in all the welds as similar welding parameters were used. Accordingly, it was expected that the CCT curve of the steel with chemistry that of the dissimilar weld would lie between the individual curve of the HSLA and DP980 steel (Fig. 7). Therefore, bainite was expected to form in the FZ of the dissimilar weld; however, the bainite volume fraction would be lower than that formed in the FZ of HSLA weld (Fig. 3). This was reflected in the hardness profiles as well. For example, the dissimilar weld FZ possessed an average hardness of 425 HV, which was close to the average hardness of the FZ of HSLA weld (415 HV). Therefore, it can be anticipated that identical FZ microstructure i.e. bainite and martensite were formed in both dissimilar and HSLA steel welds with slight high hardness in dissimilar FZ because of the richer chemistry. On the other hand, the fully martensitic microstructure in the DP980 steel FZ resulted in higher average hardness (480 HV).

4.2. TEM and nanoindentation study of bainite structure

The formation of bainite was confirmed by TEM analysis, the representative TEM micrographs of the dissimilar weld FZ are shown in Fig. 8. The microstructure well resembled the typical lower bainite sheaf (Fig. 8(a)) containing multiple variants of carbide precipitates (Fig. 8(b) and (c)) within bainitic ferrite laths [6,38]. The average lath width of bainitic ferrite was measured from images of 3–4 different regions to be about 1.5 μm. Apart from dispersion multiple variant carbides precipitate within the bainitic ferrite laths (Fig. 8(c)); plate-like carbides were formed at the bainitic ferrite lath boundaries (marked as interlath cementite/carbide in Fig. 8(b)). The selected area diffraction pattern (SADP) taken from the bainitic ferrite laths was indexed to be the $[\bar{1}11]_\alpha$ zone axis of ferrite (α) (inset of Fig. 8(c)); the lattice parameter (a) was calculated to be 2.87 Å. The dark field image (Fig. 8(d)), taken using the spot diffraction spot close to the (101) diffraction spot (indicated by the arrow) of α revealed the carbides precipitated in a single crystallographic variant within the bainitic ferrite sheaves. The d-spacing measured for this spot was indexed to be the (013) reflection of cementite.

The typical martensite microstructure observed in the FZ (Fig. 9) showed packets, which were composed of several parallel martensite laths separated by thin films of retained austenite. The martensite laths showed typical feature of martensite phase i.e. a high density of dislocations (Fig. 9(b)). TEM analysis clearly

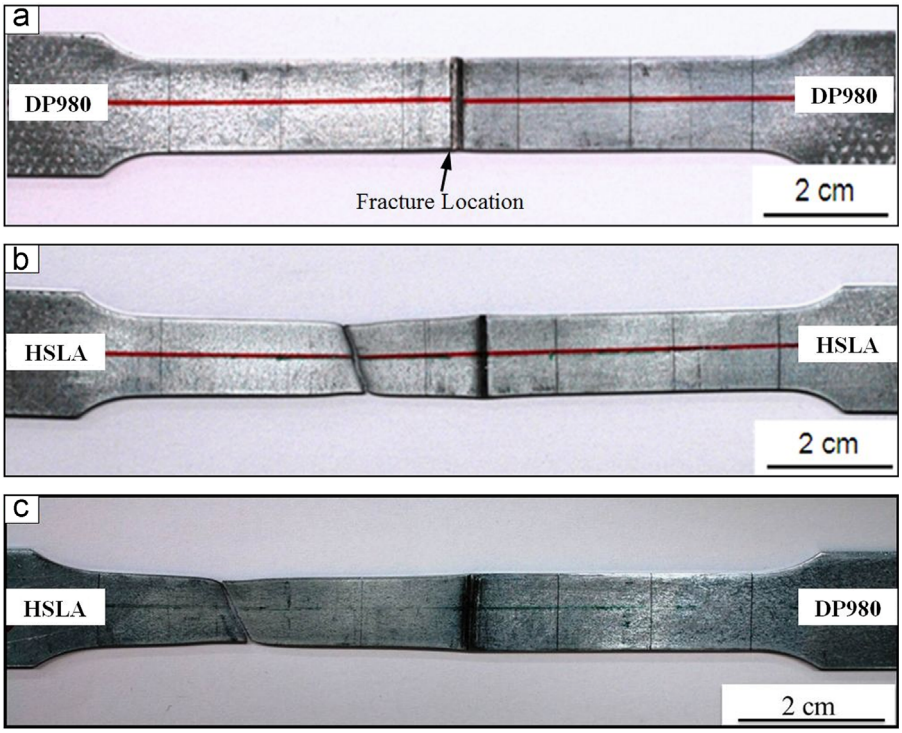

Fig. 5. Typical tensile failure locations of fiber laser welded joints: (a) DP980, (b) HSLA, and (c) dissimilar weld; produced using 6 kW and 16 m/min [14].

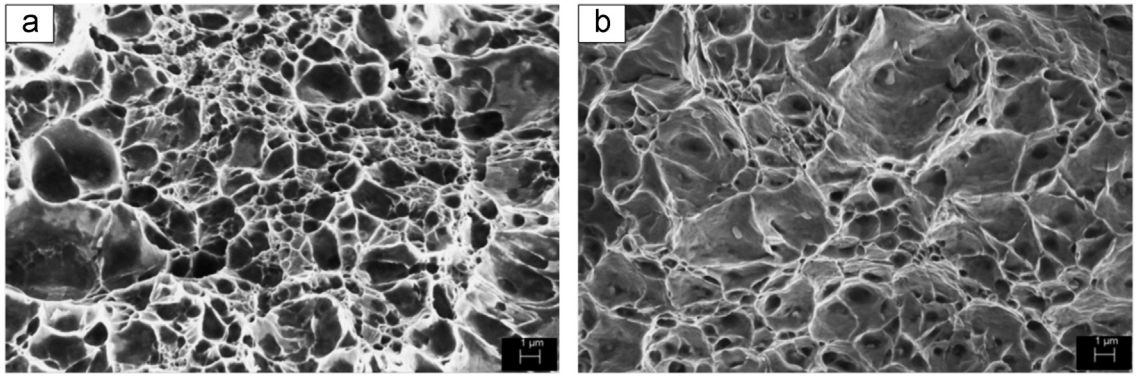

Fig. 6. SEM micrographs of the tensile fractured surface of a welded joint tested at a strain rate of 0.001/s (a) SCHAZ of DP980, and (b) HSLA BM.

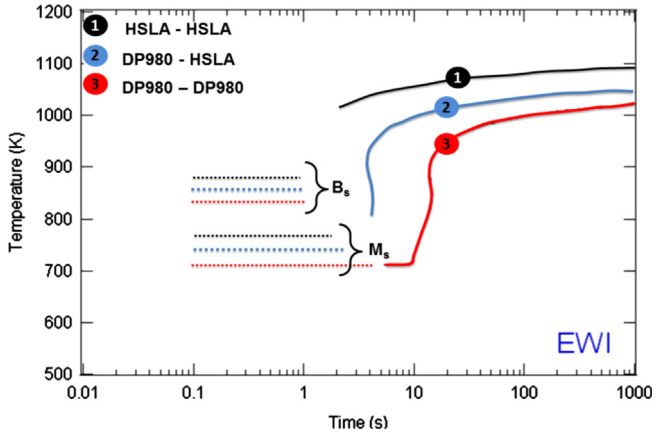

Fig. 7. CCT diagram for a representative DP980, HSLA steels, and their dissimilar combination based on the model developed by Bhadeshia and Sevensson [42].

differentiated the microstructural constituent i.e. lower bainite and martensite in Figs. 8 and 9, respectively, which were seen within the dissimilar FZ.

Further confirmation of the bainite structure observed in TEM analysis of the FZ was obtained by nanoindentation. As expected the martensite and bainite phases showed different nano-hardness within the FZ. The load–displacement curves for indents impression of the lowest (4.11 GPa, for bainite) and highest (6.57 GPa, for martensite) are presented in Fig. 10(a); and their corresponding SEM micrographs are shown in Fig. 10(b) and (c), respectively. It should be noted that SEM study indicated that the indents which spanned across both microconstituents had intermediate hardness values. The indent in Fig. 10(b) clearly indicated that the nano-hardness of the lower bainitic ferrite lath structure. The bainitic ferrite lath width in Fig. 10(b) was found to be identical (about 1.5 μm) to that observed in TEM (Fig. 8(a)). On the other hand, the impression shown in Fig. 10(c) corresponds to the martensite laths; without any contribution of grain boundaries between phases to nano-hardness. The SEM image of bainite (Fig. 10(b)) suggested that the indent on a bainitic ferrite phase shows significant plastic flow of the materials at the periphery of the indent; and also a high indentation depth can be detected in this case. In contrast to bainitic ferrite structure, indentation on finer martensite laths can resist deformation resulting in less

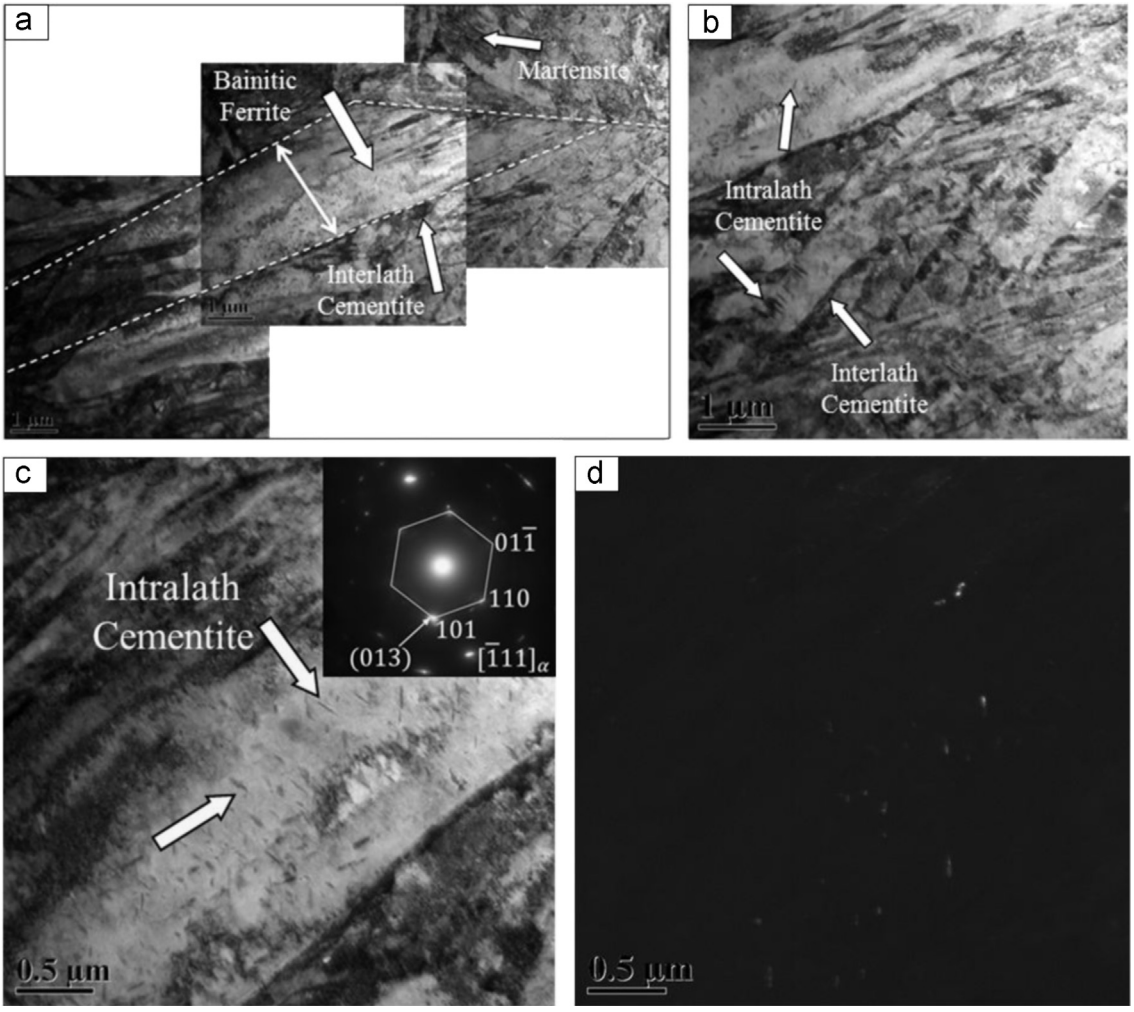

Fig. 8. Microstructure of dissimilar DP980 and HSLA FZ showing: (a) lower bainite; bainitic ferrite lath (bright region) with interlath cementite plates (dark areas), (b) another view of bainite showing inter and intralath cementite, (c) bright images of bainitic ferrite lath with intralath cementite and corresponding indexed SAD inset, (d) dark field image of (c) taken using θ-Fe_3C (013) spot confirming the cementite.

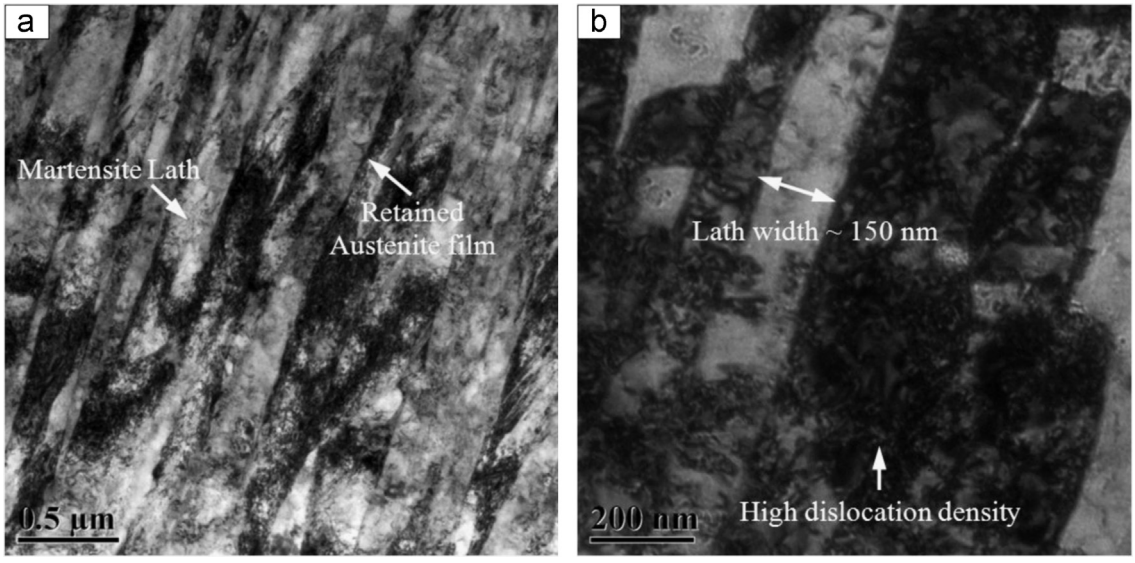

Fig. 9. Representative TEM images delineating martensite structure in the dissimilar FZ: (a) martensite laths embedded with inter-laths retained austenite films, and (b) magnified view of laths showing high dislocation density.

pile-up or excursion [39], which was consistent with the load–displacement curves for both the indents (Fig. 10(a)). The indent on martensite laths possesses the highest nano-hardness (6.57 GPa) and shows lower indent depth (136 nm) compared to bainitic ferrite counterpart (170 nm). The measured nano-hardness value of the martensite structure was close to those obtained by

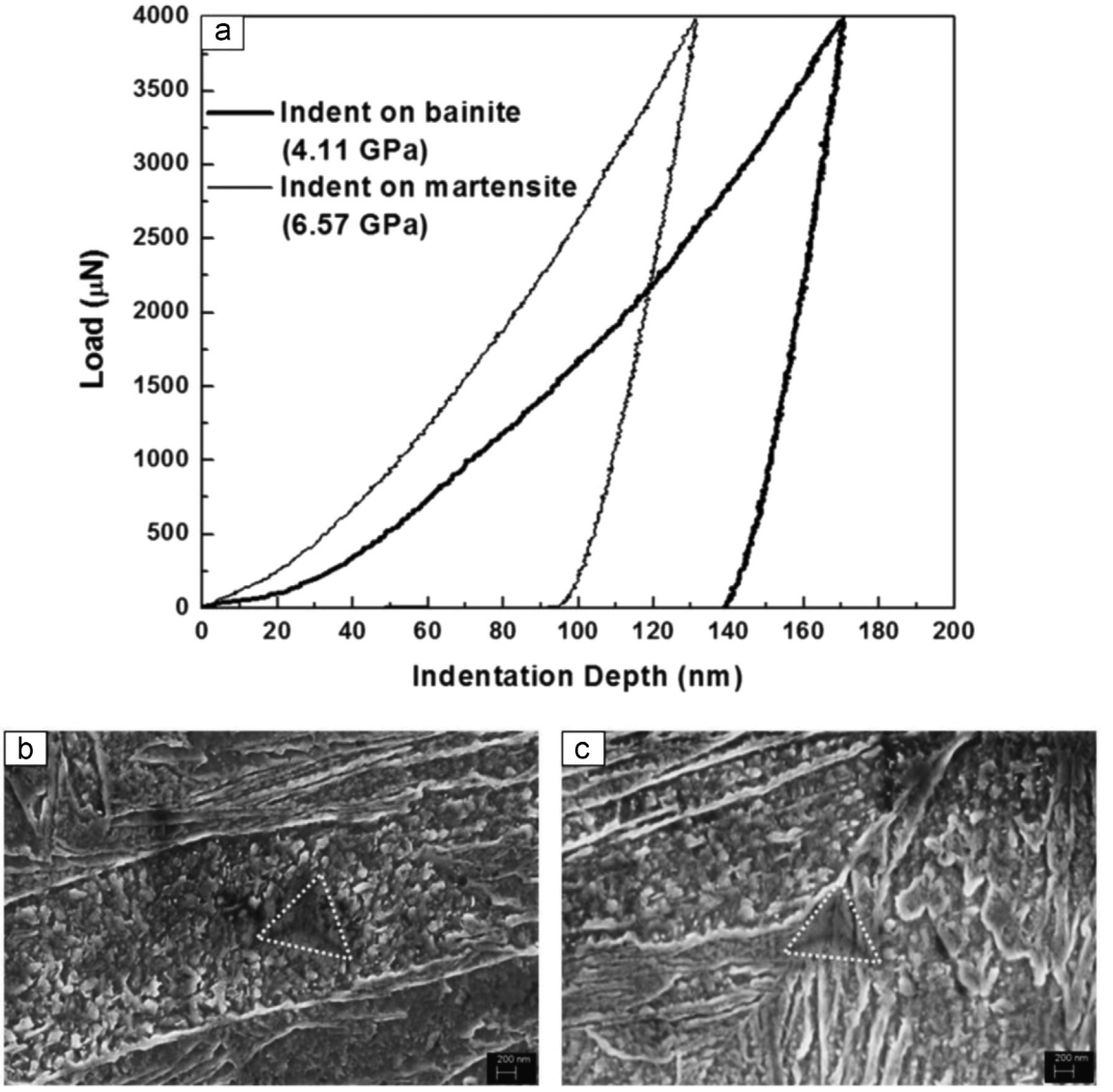

Fig. 10. Nanoindentation test results on the FZ showing, (a) load–displacement curves (*P*–*h*) corresponding to indent on bainite and martensite and (b) and (c) showing impressions for bainite and martensite, respectively.

Hernandez et al. [40]. The nano-hardness of bainite structure is reported to be 3.8–4.9 GPa [41] with the variation in the nano-hardness being strongly correlated to the intrinsic characteristics of the bainite, such as, the fraction of precipitated cementite, crystallographic orientation and the non-uniformity of the dislocation density. In the present study, nano-hardness of bainite was measured in the range of 4.11–4.53 GPa and was determined by the locations of the indents i.e. at center of the bainite or in the vicinity of the grain boundaries. Therefore, it was concluded that reduction of hardness detected near the weld centerline of dissimilar weld (Fig. 3) was due to the formation of lower bainite structure as a result of chemistry dilution.

4.3. Failure location in tensile test

The failure occurred at the SCHAZ for similar DP980 (Fig. 5(a)) where the microstructure consists of ferrite and tempered martensite (Fig. 2(b)); therefore the fracture surface shows dimpled cup-like fracture (Fig. 6(a)). The tempered martensite structure and HSLA BM microstructure were identical, having a ferrite matrix and precipitated carbides; therefore, the deformation behavior of these structures was identical leading to typical dimple morphology of ductile fracture. This can also be attributed to the close strength i.e. hardness of these two structures [40]. Hernandez et al. [40] reported that the nano-hardness of the tempered martensite and ferrite phase are close; therefore indistinguishable fracture morphologies is expected, which was observed in the present study (Fig. 6(a)). On the other hand, the fracture in the HSLA and dissimilar welds consistently occurred in the HSLA BM. Fig. 5 (b) and (c) indicated that substantial plastic deformation (necking) of the BM had occurred in the HSLA BM before failure at a certain angle to the loading direction (Fig. 5(c)). Typical ductile fracture of the HSLA steels is expected because of the microstructure dominated by the ductile ferrite matrix. The elongated dimpled structure seen in the dissimilar and HSLA welds is related to the deformation of the ferrite grains and the fine carbide precipitates acting as the crack initiation sites leading to the formation of the micro voids (Fig. 6(b)).

5. Conclusions

Fiber laser welded DP980 steel, HSLA steel, and their dissimilar combination were evaluated with respect to microstructure,

hardness, and tensile properties. Following conclusions were drawn from this study.

1. Fusion zone microstructure was sensitive to materials chemistry; lean chemistry was formed due to mixing of the two materials which resulted in the shifting of the CCT diagram to the left side. However, the hardness trend of the dissimilar weld implies that the mixing was not completed which reduces the hardenability due to inhomogeneity.
2. Hardness profile within the dissimilar weld implied that the mixing of chemistry within the FZ was not homogeneous leading to larger variation in hardness.
3. TEM study revealed that the bainite phase observed in the dissimilar FZ comprised of bainitic ferrite embedded with both intra-lath and interlath cementite precipitates. The bainite structure exhibited a lower nano-hardness (4.5 GPa), with a significant plastic flow of the materials at the periphery of the indents, comparing to martensite phase (6.57 GPa).
4. Tensile strength of the dissimilar weld were close to the HSLA welds, but lower than the DP980 steel welds, with failure consistently occurred on the HSLA base metal like in the HSLA welds. DP980 welds failed at the tempered region of the HAZ where softening was observed.

Acknowledgments

Authors would like to acknowledge International Zinc Association in Durham, NC, USA, AUTO21, Canada's Automotive Research and Development Program, and Innovation in Automotive Manufacturing Initiative (IAMI) in Canada for financing this project. Authors are thankful to ArcelorMittal Dofasco Inc. in Hamilton, Canada for providing the materials to carry out this work.

References

[1] S. Drew, F. Greg, W. Michael, C.A. Susan, D. Rita Van, Z.M. Nicholas, A. Jeff, K. Dorothy, M. George, Nat. Clim. Chang. 1 (2011) 59–66.
[2] H.-J. Kim, C. McMillan, G.A. Keoleian, S.J. Skerlos, J. Ind. Ecol. 14 (2010) 929–946.
[3] ULSAB-AVC Body Structure Materials, 2001.
[4] M.S. Rashid, Annu. Rev. Mater. Sci. 11 (1981) 245–266.
[5] M.S. Rashid, US Patent 4,129,461, 1978.
[6] R.W.K. Honeycombe, H.K.D.H. Bhadeshia, Steels: Microstructure and Properties, E. Arnold, 1981.
[7] V.H. Baltazar Hernandez, M.L. Kuntz, N.Y. Zhou, in: Proceedings of the Sheet Metal Welding Conference XIII, Livonia, MI, 2008.
[8] F.I. Saunders, R.H. Wagoner, Metall. Mater. Trans. A 27 (1996) 2605–2616.
[9] L.C. Chan, C.H. Cheng, S.M. Chan, T.C. Lee, C.L. Chow, J. Manuf. Sci. Eng. 127 (2005) 743–751.
[10] K.B. Min, S.S. Kang, J. Mater. Process. Technol. 103 (2000) 218–224.
[11] E. Keehan, Chalmers University of Technology and Goteborg University, Goteborg, Sweden, 2004.
[12] W. Xu, D. Westerbaan, S. Nayak, D. Chen, F. Goodwin, E. Biro, Y. Zhou, Mater. Sci. Eng. A 553 (2012) 51–58.
[13] W. Xu, D. Westerbaan, S. Nayak, D. Chen, F. Goodwin, Y. Zhou, Mater. Des. 43 (2013) 373–383.
[14] D. Westerbaan, S.S. Nayak, D. Parkes, W. Xu, D.L. Chen, S.D. Bhole, F. Goodwin, E. Biro, Y. Zhou, in: Proceedings of the Sheet Metal Welding Conference XV, Michigan, USA, 2012.
[15] A.S.P. Program, Tailor Welded Blank Design and Manufacturing Manual, Auto/Steel Partnership, 1995.
[16] M. Uchihara, K. Fukui, Weld. Int. 20 (2006) 612–621.
[17] H. Kusuda, T. Takasago, F. Natsumi, J. Mater. Process. Technol. 71 (1997) 134–140.
[18] M.F. Shi, G.H. Thomas, M.X. Chen, J.R. Fekete, Iron Steelmak. 29 (2002) 27–32.
[19] P. Ghosh, ISIJ Int. 30 (1990) 317–324.
[20] C. Ma, D. Chen, S. Bhole, G. Boudreau, A. Lee, E. Biro, Mater. Sci. Eng. A 485 (2008) 334–346.
[21] M. Khan, M. Kuntz, E. Biro, Y. Zhou, Mater. Trans. 49 (2008) 1629–1637.
[22] V.H. Baltazar Hernandez, S.S. Nayak, Y. Zhou, Metall. Mater. Trans. A 42 (2011) 3115–3129.
[23] A. Santillan Esquivel, S. Nayak, M. Xia, Y. Zhou, Can. Metall. Q. 51 (2012) 328–335.
[24] N. Farabi, D. Chen, Y. Zhou, J. Mater. Eng. Perform. 21 (2012) 222–230.
[25] S. Chowdhury, D. Chen, S. Bhole, E. Powidajko, D. Weckman, Y. Zhou, Metall. Mater. Trans. A 42 (2011) 1974–1989.
[26] A. Standard, Standard Test Methods for Tension Testing of Metallic Materials, 2008, 3.
[27] M. Xia, E. Biro, Z. Tian, Y.N. Zhou, ISIJ Int. 48 (2008) 809–814.
[28] N. Farabi, D. Chen, Y. Zhou, Procedia Eng. 2 (2010) 835–843.
[29] N. Sreenivasan, S. Lawson, Y. Zhou, Z. Tian, J. Eng. Mater. Technol. 129 (2007) 44–452.
[30] S.S. Nayak, V.H. Baltazar Hernandez, Y. Zhou, Metall. Mater. Trans. A 42 (2011) 3242–3248.
[31] A. Kumar, S. Singh, K. Ray, Mater. Sci. Eng. A 474 (2008) 270–282.
[32] E. Biro, A. Lee, in: Proceedings of the Sheet Metal Welding Conference XI, 2004.
[33] V.H.B. Hernandez, S.K. Panda, Y. Okita, N.Y. Zhou, J. Mater. Sci. 45 (2010) 1638–1647.
[34] E. Biro, A. Lee, in: Proceedings Sheet Metal Welding Conference XII, 2006.
[35] M. Mukherjee, T.K. Pal, Mater. Sci. Technol. 28 (2012) 343–352.
[36] J. Gould, S. Khurana, T. Li, Weld. J. 85 (2006) 111s–116s.
[37] S. Kou, Welding Metallurgy, Cambridge University Press, 2002.
[38] H.K.D.H. Bhadeshia, Bainite in Steels, Institute of Metals (1992) .
[39] K. Kese, Z.-C. Li, B. Bergman, Mater. Sci. Eng. A 404 (2005) 1–8.
[40] V. Baltazar Hernandez, S. Panda, M. Kuntz, Y. Zhou, Mater. Lett. 64 (2010) 207–210.
[41] B.-W. Choi, D.-H. Seo, J.-i. Jang, Met. Mater. Int. 15 (2009) 373–378.
[42] H.K.D.H. Bhadeshia, L.E. Svensson, Modelling the Evolution of Microstructure in Steel Weld Metal, Mathematical Modeling of Weld Phenomena, Institute of Materials, Minerals and Mining, London (1993) 109–180.